Preparation and study of 2-D semiconductors with Dirac type bands due to the honeycomb nanogeometry

Reference:

Kalesaki E., Boneschanscher M.P., Geuchies J.J., Delerue C., Morais Smith C., Evers W.H., Allan G., Altantzis Thomas, Bals Sara, Vanmaekelbergh D..- Preparation and study of 2-D semiconductors with Dirac type bands due to the honeycomb nanogeometry

Proceedings of SPIE - ISSN 0277-786X - 8991(2016), 898107

Full text (Publishers DOI): http://dx.doi.org/doi:10.1117/12.2042882

Preparation and study of 2-D semiconductors with Dirac type bands due to the honeycomb nanogeometry.

E. Kalesaki[1], M.P. Boneschanscher[2], J.J. Geuchies[2], C. Delerue [1,2], C. Morais Smith[3], W.H. Evers[4], G. Allan[1], T. Altantzis[5], S. Bals[5], and D. Vanmaekelbergh[2]

1. IEMN- Dept. ISEN, UMR CNRS 8520, Lille
2. Debye Institute for Nanomaterials Science, University of Utrecht
3. Institute for Theoretical Physics, University of Utrecht
4. Opto-electronic Materials Section, Kavli Institute of Nanoscience, Delft University of Technology
5. EMAT, University of Antwerp

Overview: 2-D semiconductors with a honeycomb nanogeometry.

The interest in 2-dimensional systems with a honeycomb lattice and related Dirac-type electronic bands has exceeded the prototype graphene[1]. Currently, 2-dimensional atomic[2,3] and nanoscale[4-8] systems are extensively investigated in the search for materials with novel electronic properties that can be tailored by geometry. *The immediate question that arises is how to fabricate 2-D semiconductors that have a honeycomb nanogeometry, and as a consequence of that, display a Dirac-type band structure?*

Here, we show that atomically coherent honeycomb superlattices of rocksalt (PbSe, PbTe) and zincblende (CdSe, CdTe) semiconductors can be obtained by nanocrystal self-assembly and facet-to-facet atomic bonding, and subsequent cation exchange. We present a extended structural analysis of atomically coherent 2-D honeycomb structures that were recently obtained with self-assembly and facet-to-facet bonding[9]. We show that this process may in principle lead to three different types of honeycomb structures, one with a graphene type-, and two others with a silicene-type structure. Using TEM, electron diffraction, STM and GISAXS it is convincingly shown that the structures are from the silicene-type.

In the second part of this work, we describe the electronic structure of graphene-type and silicene type honeycomb semiconductors. We present the results of advanced electronic structure calculations using the $sp^3d^5s^*$ atomistic tight-binding method[10]. For simplicity, we focus on semiconductors with a simple and single conduction band for the native bulk semiconductor. When the 3-D geometry is changed into 2-D honeycomb, a conduction band structure transformation to two types of Dirac cones, one for S- and one for P-orbitals, is observed. The width of the bands depends on the honeycomb period and the coupling between the nanocrystals. Furthermore, there is a dispersionless P-orbital band, which also forms a landmark of the honeycomb structure. The effects of considerable intrinsic spin-orbit coupling are briefly considered. For heavy-element compounds such as CdTe, strong intrinsic spin-orbit coupling opens a non-trivial gap at the P-orbital Dirac point, leading to a quantum Spin Hall effect[10-12].

Our work shows that well known semiconductor crystals, known for centuries, can lead to systems with entirely new electronic properties, by the simple action of nanogeometry. It can be foreseen that such structures will play a key role in future opto-electronic applications, provided that they can be fabricated in a straightforward way.

Physics, Simulation, and Photonic Engineering of Photovoltaic Devices III, edited by Alexandre Freundlich, Jean-François Guillemoles, Proc. of SPIE Vol. 8981, 898107 · © 2014 SPIE
CCC code: 0277-786X/14/$18 · doi: 10.1117/12.2042882

Preparation of 2-D semiconductors with a honeycomb nanogeometry

Oriented attachment is a process in which two adjacent nanocrystals form a single one, due to an atomically matched bond formation between two specific facets[13,14]. Controlled oriented attachment is currently emerging as a route to form extended one- and two-dimensional single-crystalline semiconductors of II-VI and IV-VI compounds[9,15-17]. These systems are of large interest in opto-electronics, and are commonly fabricated by expensive gas-phase methods.

Honeycomb semiconductors composed of PbSe. With truncated nanocubes of the Pb-chalcogenide family, 2-D atomically coherent ultra-thin quantum wells as well as superlattices with astounding square or honeycomb nanogeometry have been recently reported[9]. The formation of such systems is highly remarkable, as several demanding conditions have to be fulfilled: the nanocrystal building blocks must be nearly monodisperse in size and shape, and attachment should only occur with a geometrically defined subset of nanocrystal facets of one sort. The amazing atomic and nanoscale order in such systems is far from understood. This is most obvious for extended, atomically coherent PbSe superlattices with honeycomb nanogeometry. In this case, immediate questions on the large-scale crystallographic orientation of the nanocrystals, the release of the capping at specific facets, and the atomic mechanism of attachment emerge. We now present a detailed structural analysis of these systems using methods in real and wave vector space. This analysis also shines light on the mechanism of the self-assembly, the long-range orientation of the nanocrystals before attachment, and the microscopic mechanism of the attachment process.

Figure 1 presents the honeycomb structure obtained by oriented attachment of PbSe nanocrystal building blocks. The initial building blocks have the shape of a truncated cube terminated with [100], [110], and [111] facets. To estimate the nanoparticle size we determined the radially averaged diameter of the TEM projections, and found this to be 5.4 ± 0.4 nm. The oriented attachment of these nanoparticles results in structures with long-range periodicity, as visualized by means of an equilateral triangle in the HAADF-STEM image (Figure 1A). Furthermore the structures have a high degree of crystallinity, as observed by means of electron diffraction (Figure 1C). Zooming in on the honeycomb structure (Figure 1B) reveals that the [111] facets of the nanocrystals are parallel to the honeycomb plane, and that the symmetry axes of this facet (i.e., the [1-10] atomic planes) are aligned with the nanocrystal-nanocrystal bonds. This is also corroborated by the recorded electron diffraction patterns (Figure 1C).

At this point we can assume three different models for attachment of the nanocrystals that result in a honeycomb structure with the nanocrystal [111] facets parallel to the honeycomb plane, being attachment via the [110], [111], or [100] facets, respectively (Figure 1D-I). The three models look similar from the top, but have a very different 3D shape. The first model is a planar, trigonal structure with bond angles between the nanocrystals of 120^{o} (Figure 1D,E). The second model is slightly buckled, with tetrahedral symmetry and nanocrystal bond angles of 109.5^{o} (Figure 1F,G). The third model is highly buckled, with octahedral symmetry and nanocrystal bond angles of 90^{o} (Figure 1H,I). The trigonal model, where attachment takes place via the [110] facets, requires that the [1-10] atomic planes are under a 30^{o} angle with the nanocrystal-nanocrystal bonds. This is visible in Figure 1D in the pointing away of the [110] facets from the nanocrystal-nanocrystal bonds. However, both the high-resolution HAADF-STEM images and the electron diffraction patterns show that the [1-10] atomic planes are aligned with the nanocrystal bonds, allowing to quickly discard this model. Another indication that the honeycomb structure is buckled is observed in the HAADF-STEM images where the additional scattering strength on the nanocrystal bonds indicates a larger than average thickness of the sample. However, both the tetrahedral and octahedral model are buckled and have the [1-10] atomic planes aligned with the honeycomb nanogeometry, making it impossible to discriminate between the two on basis of high resolution HAADF-STEM or electron diffraction.

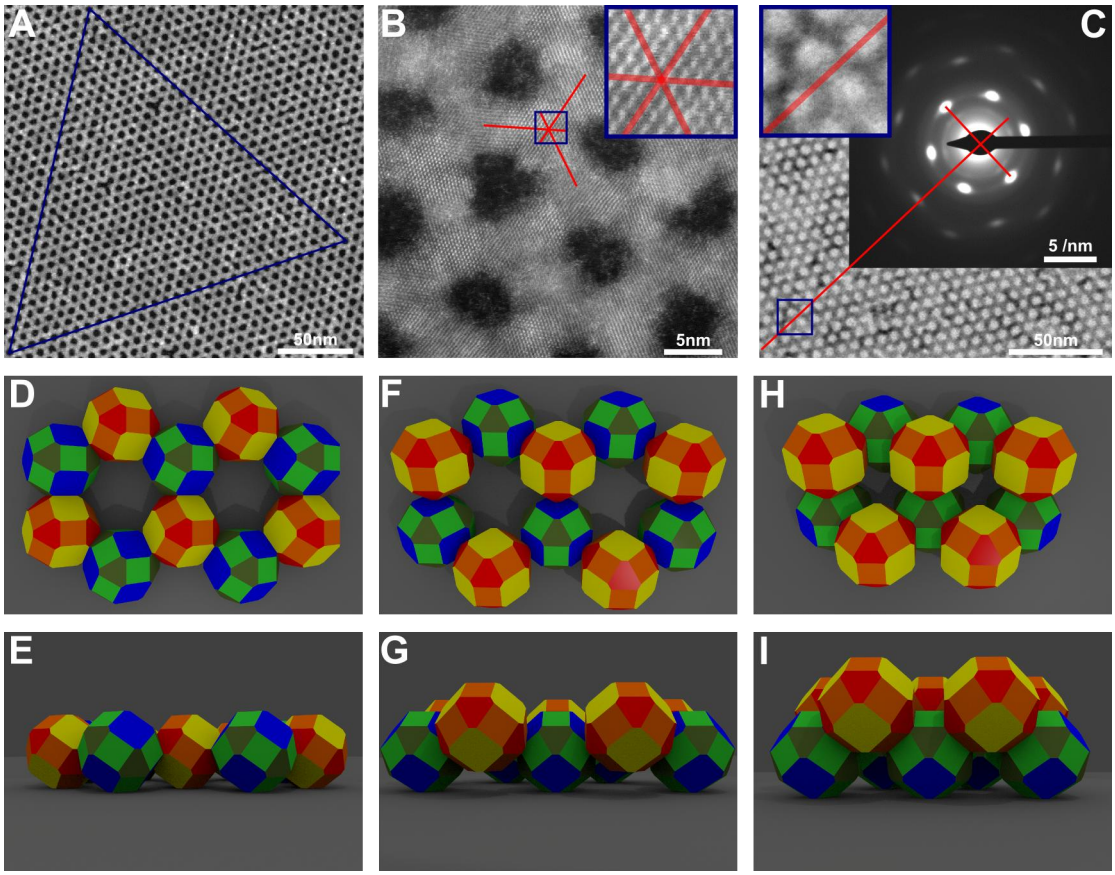

Figure 1. Single crystalline PbSe honeycomb structures created by oriented attachment. A) HAADF-STEM image of the honeycomb structure. The equilateral triangle shows the long-range ordering of the structure. B) High resolution HAADF-STEM image showing that the [111] facets are parallel to the substrate, and that the symmetry axes of these facets are aligned with the nanocrystal-nanocrystal bonds. C) Electron diffraction pattern showing the high degree of crystallinity. The first ring of clear diffraction spots originates from the [2-20] atomic planes. The orientation of the diffraction spots with respect to the real space TEM image confirms that these planes are parallel to the nanocrystal-nanocrystal bonds. D-I) Models of the honeycomb structure with truncated cubes for the nanocrystals. The two inequivalent sites in the honeycomb lattice are indicated by yellow/red nanocrystals and blue/green nanocrystals. The triangles (red, dark green) are the [111] facets, the rectangles (orange, light green) are the [110] facets, and the squares (yellow, blue) are the [100] facets of the nanocrystals. (D,E) Top and side view of the trigonal structure. (F,G) Top and side view of the tetrahedral structure. (H,I) Top and side view of the octahedral structure.

The ability to discriminate between the tetrahedral and octahedral honeycomb structure is essential for both understanding the oriented attachment process as well as modelling the electric properties of the honeycomb structure. Here, we use a combination of scanning tunnelling microscopy (STM) and grazing-incidence small-angle X-ray scattering (GISAXS) to fully resolve the honeycomb structure. (Figure 2). We can extract the next-nearest neighbour (NNN) distances from STM and find these to be 8.5 ± 0.8 nm. In GISAXS we find scattering peaks arising from the hexagonal order of the holes in the honeycomb structure with relative positions of 1: $\sqrt{3}$:2: $\sqrt{7}$, as expected from a honeycomb structure (Figure 2). Looking at the absolute peak positions we find a hole-hole distance of 8.5 nm, in accordance with the NNN distances observed in STM. Assuming perfect honeycomb models, this distance would correspond to a bond length of 5.2 nm for the tetrahedral and 6.0 nm for the octahedral honeycomb structure. Hence, the above results strongly indicate that our structures have the octahedral honeycomb nanogeometry. This is corroborated by recent HAADF-STEM tomography, discussed elsewhere.

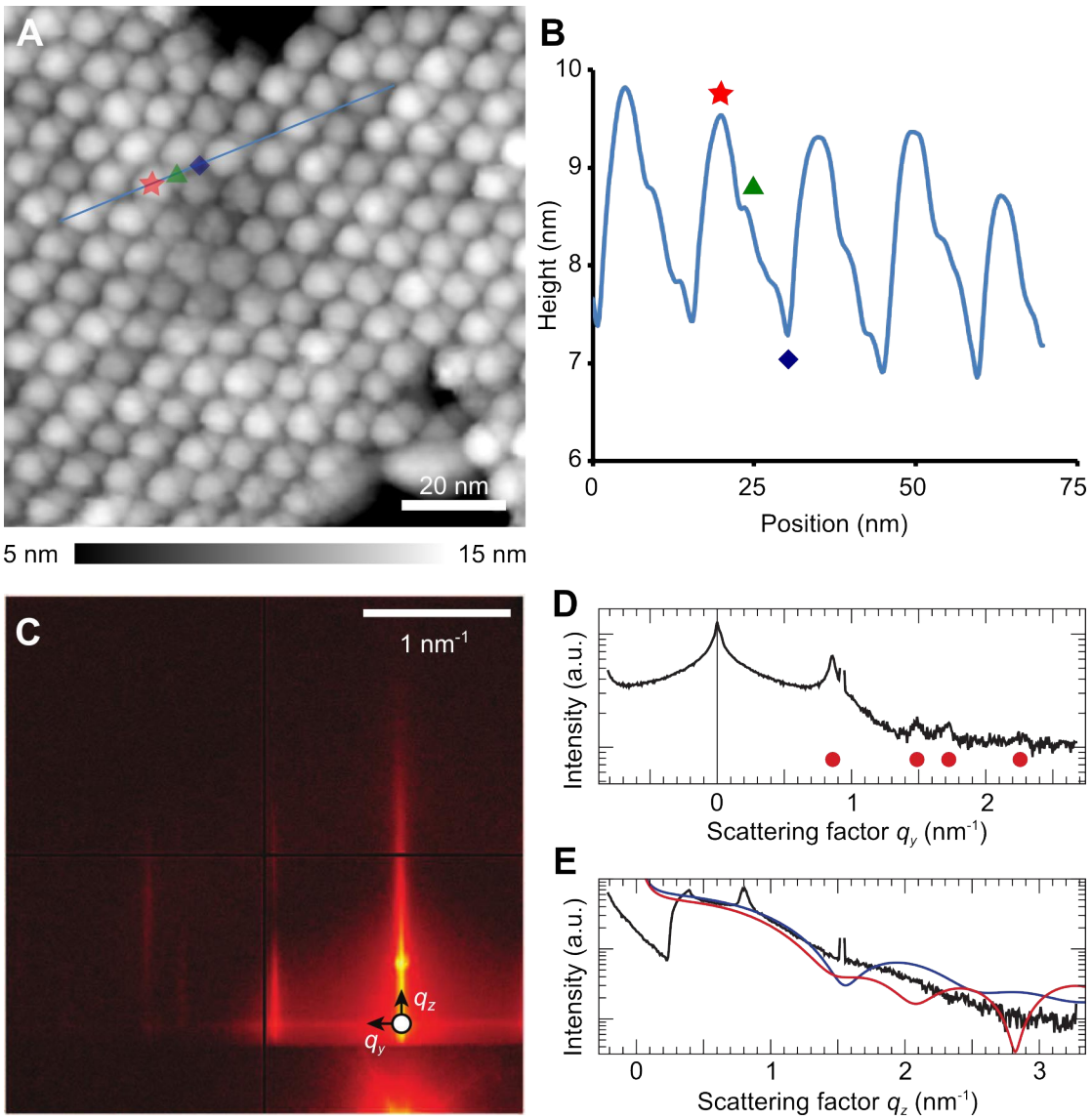

Figure 2. STM and GISAXS measurements on the PbSe honeycomb structures. (A) STM topography showing that the nanocrystals are at different height. (B) Height profile along the blue line indicated in (A). The position of a high nanocrystal (star), low nanocrystal (triangle), and hollow site (diamond) are indicated. (C) GISAXS pattern a honeycomb structure on top of a Si(100) substrate, under an angle of incidence of 0.7 degrees. (D) Line trace in the horizontal direction indicated in (C), revealing the in-plane order. Red disks mark diffraction peaks with relative positions of 1: $\sqrt{3}$:2: $\sqrt{7}$, arising from the hexagonal order of the holes in the structure. This corresponds to bond lengths of either 5.18 nm for the tetrahedral honeycomb structure, or 6.00 nm for the octahedral honeycomb structure. (E) Line trace in the vertical direction indicated in (C), representing the electron density profile in the direction normal to the surface. The Fourier transform of the electron density profile calculated for the tetrahedral honeycomb (blue) structure and for the octahedral honeycomb structure (red). From the vertical and horizontal line traces, it can be concluded that the structures that are formed are silicene-type honeycombs, of the octahedral type (see Fig. 1 H, I).

Above, we have shown that the honeycomb structures attach via the [100] facets into a structure with octahedral symmetry. We now reconsider the bond lengths of the honeycomb structure, as extracted from TEM, STM, GISAXS, and

tomography. All four techniques give an independent measure of 6.0 nm for the nanocrystal bond lengths, an increase of 10% of the original nanocrystal diameter. The increased bond lengths shine light on the microscopic mechanism of facet-to-facet atomic attachment. D. Li et al.[14] showed that, in the process of oriented attachment, the nanocrystals are continuously rotating and moving in close proximity by means Brownian motion, in this way trying to find an optimum configuration before enduring attachment takes place. Our results show that two facing nanocrystals can be separated by about half a nanometer after the attachment. We therefore propose the following mechanism for oriented attachment of organically capped nanocrystals in apolar media: during the rotation and Brownian motion as described by D. Li et al.[14], atomic scale necking takes place as a first step in the attachment. After necking has started, the capping molecules can be gradually removed and the neck extends perpendicular to the bond axis by vast atomic motion. For PbSe nanocrystals considerable atomic reconfigurations have been monitored by high resolution TEM in vacuum[18-20]. The necking explains the elongation of the bond lengths, which also results in considerably more open honeycomb structure than can be obtained from geometric attachment of rigid block models (compare Figure 1H with the real structures in Figures 1 and 3). In this necking mechanism, not all the capping molecules have to be released at once from a facet, allowing for attachment pathways with lower activation energy.

Honeycomb semiconductors composed of zinc blende CdSe. An important question is if the formation of 2-D honeycomb structures is limited to Pb-chalcogenide materials or not? It should be remarked that the specific shape of the building blocks – *rock salt* nanocrystals with a *truncated cubic shape* - is a key element in the formation of the honeycomb structures. The tight-binding calculations predict Dirac conduction bands, if the inherent conduction band structure is a simple parabolic band, as for zinc blende. For this reason, we have attempted to fabricate honeycomb semiconductors of CdSe with a zinc blende atomic structure, using Cd-for-Pb ion exchange.

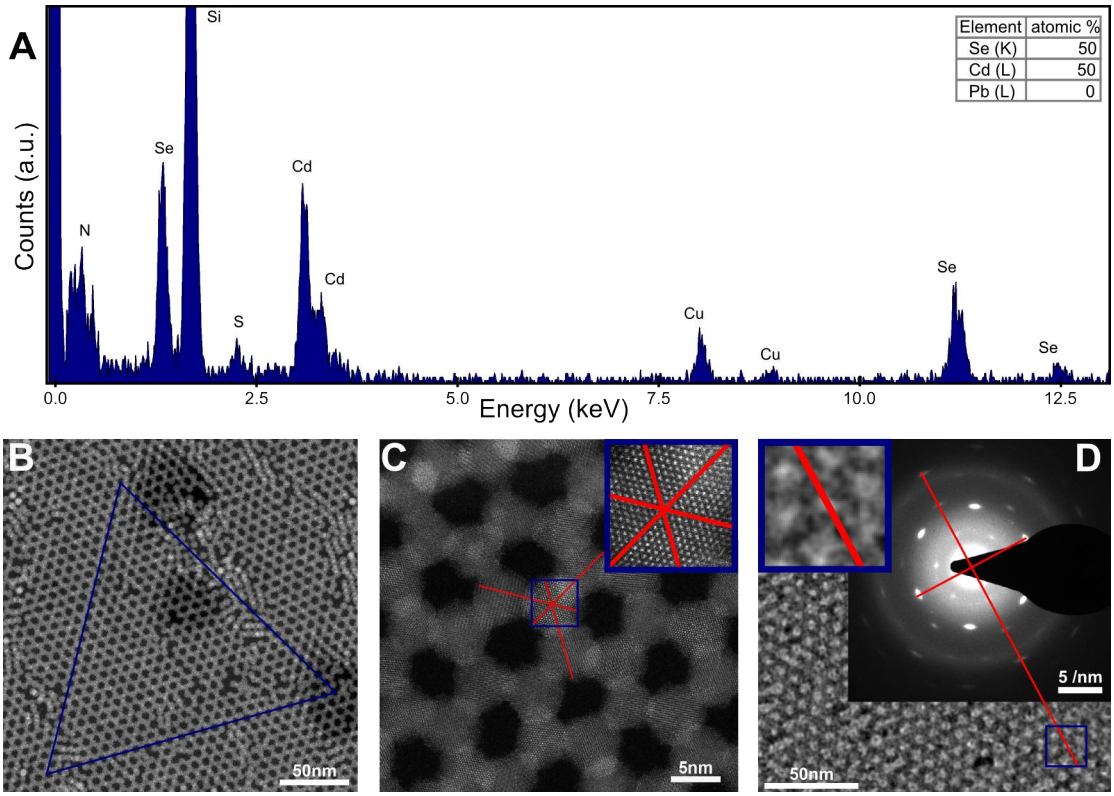

Figure 3. Single crystalline CdSe honeycomb structures created by cation exchange. A) Energy-dispersive X-ray spectrum of the CdSe honeycomb structure, showing a total absence of Pb and a 1:1 ratio of Cd:Se. B) HAADF-STEM image of the CdSe honeycomb structure. The equilateral triangle shows that the long range ordering of the structure is retained. C) High resolution HAADF-STEM image showing that orientation of the Se anion lattice with respect to the nanogeometry is preserved. D) Electron diffraction pattern showing that the high degree of crystallinity is preserved. The orientation of the diffraction spots with respect to the real space TEM image confirms that the [1-10] facets are oriented along the nanocrystal-nanocrystal bond axis.

Figure 3 presents the successful exchange of our PbSe honeycomb lattices into CdSe. The complete transformation of the PbSe lattice into CdSe is confirmed by means of energy-dispersive X-ray spectroscopy (Figure 3A). HAADF-STEM and electron diffraction measurements show that the orientation of the Se anion lattice with respect to the honeycomb periodicity is preserved (Figure 3B-D). This is in line with earlier described mechanisms where the anion lattice is preserved during cation exchange[21,22], and is corroborated by high resolution HAADF-STEM measurements of honeycomb structures at intermediate stages of cation exchange (not shown).

Dirac conduction bands in honeycomb semiconductors

Based on the effective mass approach, Dirac-type bands of considerable width can be expected for semiconductors with a honeycomb nanogeometry[5]. However, a detailed understanding of the electronic structure and the effects of spin-orbit coupling, in relation to the atomic structure and nanoscale geometry of these systems requires more advanced calculation methods beyond the "artificial atom" approach. We have, therefore, calculated the energy bands of honeycomb superlattices composed of rock salt PbSe (PbTe) and zinc blende CdSe (CdTe) using an atomistic semi-empirical tight-binding method applied to realistic atomic configurations. In the foregoing section we reviewed that the self-assembly and attachment of truncated nanocrystal cubes may result in three different types of honeycomb structures, either with the nanocrystals in plane (i.e. a graphene type structure), or buckled, i.e. with the two sub-lattices at a different height (silicene type). For this reason, we present results for both types of honeycomb superlattices. Each atom in the superlattice is described by a double set of $sp^3d^5s^*$ atomic orbitals including the spin degree of freedom. We include spin-orbit interaction and we use tight-binding parameterizations that give very accurate band structures for bulk PbSe, CdSe and CdTe.

The electronic structure of the superlattices is always composed of a succession of several mini-bands and mini-gaps due to the honeycomb nanogeometry of the superlattice. The band structure of the PbSe superlattices is clouded due to inter-valley coupling. In the following, we discuss the simpler case in which the native 3-D semiconductor has a simple single conduction band. This is, for instance, the case for the honeycomb semiconductors composed of CdSe that we could prepare from a PbSe honeycomb lattice by Cd-for-Pb cation exchange (see above). The conduction band of CdSe (CdTe) superlattices (Figure 4a, b) is always composed of two well-separated manifolds of two and six bands (four and twelve bands including spin). In graphene-type superlattices, these bands are connected just at the K and K' points of the Brillouin zone where the dispersion is linear (Dirac points). In the second manifold higher in energy, four bands have a small dispersion and two others form very dispersive Dirac bands. The presence of Dirac points at two different energies is remarkable; it can be understood from the electronic structure of individual CdSe (CdTe) nanocrystals characterized by a spin-degenerate electron state with a 1S envelope wave-function and by three spin-degenerate 1P excited states higher in energy. The two manifolds of bands arise from the inter-nanocrystal coupling between these 1S and 1P states, respectively. Interestingly, with this nanoscale geometry, the coupling between nanocrystal wave-functions is strong enough to form dispersive bands with high velocity at the Dirac points, but small enough to avoid mixing (hybridization) between 1S and 1P states. Similar results are reached with an effective mass theory applied to a hexagonal array of repulsive gates that act on a 2-D electron gas[8], and we should remark that this simple model provides generic insight.

A fingerprint of the electronic states at the Dirac cones in graphene is their chirality with respect to a pseudo-spin associated with the two components of the wave-function on the two atoms of the unit-cell[1]. We have proved that also in the case of the nanocrystal honeycomb superlattices, the pseudo-spin is well defined near the Dirac points for all atoms on both sites of the honeycomb superlattice[10] (result not shown).

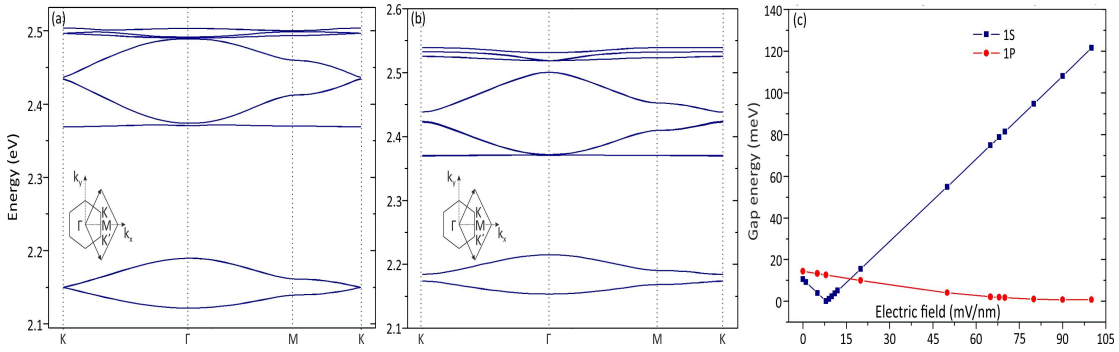

Figure 4 | Conduction bands of atomically coherent graphene-type and silicene-type honeycomb superlattices of the compound CdSe.

a, First 8 conduction bands in a K-Γ-M-K representation for the graphene-type superlattice made of truncated nanocubes with a body diagonal of 4.30 nm. The first two bands formed by nanocrystal 1S orbitals present a Dirac cone. Bands 4 and 5 give rise to a second Dirac cone, derived from the nanocrystal 1P orbitals. The third band and the top bands formed by the nanocrystal 1P orbitals are nearly dispersionless due to the geometry ($1P_{x,y}$) or weak coupling ($1P_z$). **b**, Same for the silicene-type superlattice (truncated nanocube diagonal = 5.27 nm). **c**, For the silicene lattice: evolution of the gap at K between the 1S (blue squares) and between the 1P (red circles) Dirac bands versus the electric field strength applied perpendicular to the honeycomb plane.

In the case of the graphene superlattice, the 1S and 1P bands are always characterized by well-defined Dirac points. At G, the width of the 1S band increases with decreasing nanocrystal size and increasing number of contact atoms. We predict a bandwidth above 100 meV for realistic configurations. Note that the width of the Dirac 1P bands is even considerably larger than that of the 1S bands. For artificial silicene superlattices there are gaps with varying width at the K points (Figure 2b) due to the absence of mirror symmetry with respect to the [111] contact plane between neighbour nanocrystals. However, it is shown in Figure 4c that these gaps can be (almost) completely closed by application of an electric field perpendicular to the honeycomb plane. The systematic presence of nearly flat 1P bands is another remarkable consequence of the absence of S-P hybridization. The existence of dispersionless bands has been predicted in honeycomb optical lattices of cold atoms with *p* orbitals[23,24]. In our case, two 1P bands are built from the $1P_z$ states perpendicular to the lattice, they are not very dispersive simply because $1P_z$-$1P_z$ (p-p) interactions are weak. Two other 1P bands ($1P_{x,y}$) are flat due to destructive interferences of electron hopping induced by the honeycomb geometry[23,24].

The original proposal for the realization of the quantum spin Hall effect in graphene[25], has triggered a flurry of experimental and theoretical studies[26]. Here, we show that by using heavy elements that results in strong intrinsic spin-orbit coupling, it is possible to engineer honeycomb nanocrystal superlattices that exhibit a non-trivial gap of considerable magnitude. Especially for CdTe, our calculations show a considerable gap of several meV at the K point in the 1P Dirac bands and the emergence of dispersionless edge states (manuscript in preparation). This effect is almost totally absent in real graphene, for which the intrinsic spin-orbit coupling is ~50 μeV[1].

Future experimental study of the band structure.

Numerous directions are open for the experimental investigation of these systems. The electronic structure and carrier transport can be studied by local scanning tunnelling microscopy and spectroscopy, and in a field-effect transistor geometry. With illumination and/or gating the conduction band can be controllably filled with electrons up to several electrons per nanocrystal[33] allowing for the Fermi-level to cross the Dirac points. We also should remark that the physics of honeycomb lattices of *p* orbitals with strong spin-orbit coupling is completely unexplored. Our work provides evidence for a non-trivial dispersionless P-band that can be reached at a nanocrystal filling between 2 and 3 electrons. Electron-electron interactions should then play a crucial role and may lead to Wigner crystallization[23] or to the long sought realization of fractional Chern insulators or the fractional quantum-spin Hall effect[27].

ACKNOWLEDGEMENTS

This work has been supported by funding of the French National Research Agency [ANR, (ANR-09-BLAN-0421-01)], NWO and the Dutch organization FOM [Programs "Control over Functional Nanoparticle Solids" (FNPS) and "Designing Dirac Carriers in Semiconductors".

REFERENCES

1 Castro Neto, A. H., Guinea, F., Peres, N. M. R., Novoselov, K. S. & Geim, A. K. The electronic properties of graphene. *Reviews of Modern Physics* **81**, 109-162 (2009).
2 De Padova, P. *et al.* Evidence of graphene-like electronic signature in silicene nanoribbons. *Applied Physics Letters* **96**, 261905(2010).
3 Vogt, P. *et al.* Silicene: Compelling Experimental Evidence for Graphenelike Two-Dimensional Silicon. *Physical Review Letters* **108**, 155501 (2012).
4 Tan, L. Z., Park, C.-H. & Louie, S. G. New Dirac Fermions in Periodically Modulated Bilayer Graphene. *Nano Letters* **11**, 2596-2600 (2011).
5 Park, C.-H. & Louie, S. G. Making Massless Dirac Fermions from a Patterned Two-Dimensional Electron Gas. *Nano Letters* **9**, 1793-1797 (2009).
6 Singha, A. *et al.* Two-Dimensional Mott-Hubbard Electrons in an Artificial Honeycomb Lattice. *Science* **332**, 1176-1179 (2011).
7 Gibertini, M. *et al.* Engineering artificial graphene in a two-dimensional electron gas. *Physical Review B* **79**, 241406 (2009).
8 Nadvornik, L. *et al.* From laterally modulated two-dimensional electron gas towards artificial graphene. *New Journal of Physics* **14**, 053002 (2012).
9 Evers, W. H. *et al.* Low-Dimensional Semiconductor Superlattices Formed by Geometric Control over Nanocrystal Attachment. *Nano Letters* **13**, 2317-2323 (2013).
10 Kalesaki, E., Delerue, C., Morais Smith, C., Allan, G. & Vanmaekelbergh, D. Dirac cones, topological edge states and non-trivial flatbands in two-dimensional semiconductors with a honeycomb nano-geometry. *PRX, januari 2014* (2013).
11 Kane, C. L. & Mele, E. J. Z(2) topological order and the quantum spin Hall effect. *Physical Review Letters* **95**, 146802 (2005).
12 Konig, M. *et al.* Quantum spin hall insulator state in HgTe quantum wells. *Science* **318**, 766-770 (2007).
13 Banfield, J. F., Welch, S. A., Zhang, H. Z., Ebert, T. T. & Penn, R. L. Aggregation-based crystal growth and microstructure development in natural iron oxyhydroxide biomineralization products. *Science* **289**, 751-754 (2000).
14 Li, D. *et al.* Direction-Specific Interactions Control Crystal Growth by Oriented Attachment. *Science* **336**, 1014-1018 (2012).
15 Cho, K.-S., Talapin, D. V., Gaschler, W. & Murray, C. B. Designing PbSe Nanowires and Nanorings through Oriented Attachment of Nanoparticles. *Journal of the American Chemical Society* **127**, 7140-7147 (2005).
16 Koh, W. K., Bartnik, A. C., Wise, F. W. & Murray, C. B. Synthesis of Monodisperse PbSe Nanorods: A Case for Oriented Attachment. *Journal of the American Chemical Society* **132**, 3909-3913 (2010).
17 Schliehe, C. *et al.* Ultrathin PbS Sheets by Two-Dimensional Oriented Attachment. *Science* **329**, 550-553 (2010).

18 Schapotschnikow, P., van Huis, M. A., Zandbergen, H. W., Vanmaekelbergh, D. & Vlugt, T. J. H. Morphological Transformations and Fusion of PbSe Nanocrystals Studied Using Atomistic Simulations. *Nano Letters* **10**, 3966-3971 (2010).
19 van Huis, M. A. *et al.* Atomic Imaging of Phase Transitions and Morphology Transformations in Nanocrystals. *Advanced Materials* **21**, 4992 (2009).
20 van Huis, M. A. *et al.* Low-Temperature Nanocrystal Unification through Rotations and Relaxations Probed by in Situ Transmission Electron Microscopy. *Nano Letters* **8**, 3959-3963 (2008).
21 Pietryga, J. M. *et al.* Utilizing the Lability of Lead Selenide to Produce Heterostructured Nanocrystals with Bright, Stable Infrared Emission. *Journal of the American Chemical Society* **130**, 4879-4885 (2008).
22 Casavola, M. *et al.* Anisotropic Cation Exchange in PbSe/CdSe Core/Shell Nanocrystals of Different Geometry. *Chemistry of Materials* **24**, 294-302 (2011).
23 Wu, C., Bergman, D., Balents, L. & Sarma, S. D. Flat bands and Wigner crystallization in the Honeycomb optical lattice. *Physical Review Letters* **99**, 070401 (2007).
24 Sun, K., Gu, Z., Katsura, H. & Das Sarma, S. Nearly Flatbands with Nontrivial Topology. *Physical Review Letters* **106**, 236803 (2011).
25 Kane, C. L. & Mele, E. J. Quantum spin Hall effect in graphene. *Physical Review Letters* **95**, 226801 (2005).
26 Hasan, M. Z. & Kane, C. L. Colloquium: Topological insulators. *Reviews of Modern Physics* **82**, 3045-3067 (2010).
27 Goerbig, M. O. From fractional Chern insulators to a fractional quantum spin hall effect. *European Physical Journal B* **85** (2012).